phy and single-photon emission computed tomography imaging of the dopamine transporters. *J Med Chem* 1994;37:1558–1561.
11. Baldwin RM, Zea-Ponce Y, Al-Tikriti MS, et al. Regional brain uptake and pharmacokinetics of [^{123}I]N-ω-2b-carboxy-3b-(4-iodophenyl) nortropane esters in baboons. *Nucl Med Biol* 1995;22:214–219.
12. DeKeyser J, De Baecker J, Ebinger V, Vauquelin G. Tritiated GBR 12935 binding to dopamine uptake sites in the human brain. *J Neurochem* 1989;53:1400–1404.
13. Laruelle M, Vanisberg M-A, Maloteaux J-M. Regional and subcellular localization in human brain of [^{3}H]paroxetine binding, a marker of serotonin uptake sites. *Biol Psychiatry* 1988;24:299–309.
14. Kessler RM, Ansari MS, de Paulis T, et al. High affinity dopamine D_2 receptor radioligands. 1. Regional rat brain distribution of iodinated benzamides. *J Nucl Med* 1991;32:1593–1600.
15. Farde L, Halldin C, Müller L, Suhara T, Karlsson P, Hall H. PET study of [^{11}C]β-CIT binding to monoamine transporters in the monkey and human brain. *Synapse* 1994;16:93–103.
16. Frost JJ, Rosier AJ, Reich SG, et al. Positron emission tomography imaging of the dopamine transporters with ^{11}C-WIN35,428 reveals marked declines in mild Parkinson's disease. *Ann Neurol* 1993;34:423–431.
17. Farde L, Hall H, Ehrin E, Sedvall G. Quantitative analysis of D2 dopamine receptor binding in the living human brain by PET. *Science* 1986;231:258–261.
18. Abi-Dargham A, Laruelle M, Seibyl J, et al. SPECT measurement of benzodiazepine receptors in human brain with [^{123}I]iomazenil: kinetic and equilibrium paradigms. *J Nucl Med* 1994;35:228–238.

Abnormal Cerebral Glucose Metabolism in HIV-1 Seropositive Subjects with and without Dementia

David A. Rottenberg, John J. Sidtis, Stephen C. Strother, Kirt A. Schaper, Jon R. Anderson, Mary J. Nelson and Richard W. Price

PET Imaging, Neurology and Diagnostic Radiology Services, Minneapolis VA Medical Center, and Departments of Neurology and Radiology, University of Minnesota, Minneapolis, Minnesota

This study was undertaken in order to extend our previous finding of relative basal ganglia hypermetabolism in AIDS dementia complex (ADC) and to develop clinically useful metabolic indices of CNS involvement in HIV-seropositive (HIV+) subjects. **Methods:** Twenty-one HIV+ subjects (11 with AIDS) underwent FDG-PET scanning; 12 had a follow-up scan at 6 mo and 4 had a third scan at 12 mo. Forty-three age-matched heterosexual volunteers served as controls. FDG-PET scanning was performed with arterial blood sampling, and scan data were analyzed using the Scaled Subprofile Model (SSM) with principal component analysis. **Results:** SSM/principal component analysis of the combined (HIV+ and controls) FDG-PET dataset extracted two major disease-related metabolic components: (a) a nonspecific indicator of cerebral dysfunction, which was significantly correlated with age, cerebral atrophy and ADC Stage and (b) the striatum, which was heavily weighted (relatively hypermetabolic) and appeared to provide a disease-specific measure of early CNS involvement. **Conclusion:** FDG-PET scans provide quantitative measures of abnormal functional connectivity in HIV-seropositives—with or without AIDS or ADC. These measures, which are robust across centers with respect to instrumentation, scanning technique and disease severity, appear to track the progression of CNS involvement in patients with subclinical neurologic or neuropsychologic dysfunction.

Key Words: human immunodeficiency virus; fluorine-18-fluorodeoxyglucose; PET; scaled subprofile model

J Nucl Med 1996; 37:1133–1141

The clinical features of the AIDS dementia complex (ADC) are included within the definition of subcortical dementia proposed by Albert et al. (*1*) and elaborated by Cummings and Benson (*2*). Inattentiveness, loss of spontaneity, psychomotor retardation, reduced motor performance and incoordination are the clinical hallmarks of ADC (*3–5*). Focal collections of macrophages and multinucleated giant cells in subcortical white matter and deep gray nuclei, particularly in the putamen, constitute ADC's neuropathological substrate (*4,6–8*).

In an earlier FDG-PET study, we described a metabolic covariance pattern in ADC patients, in which the basal ganglia and thalamus were relatively hypermetabolic and for which individual subject weights were highly correlated with neuropsychological test scores (*9*). We hypothesized that this covariance pattern represents a network or system of functionally interconnected brain regions involved in the production and/or expression of subcortical dementia. Our finding of relative hypermetabolism in the basal ganglia and thalamus was subsequently confirmed by van Gorp et al. (*10*) in an FDG-PET study of 17 subjects with AIDS. The current study was undertaken in an effort to extend our previous findings in a larger population of HIV-seropositives, both symptomatic and asymptomatic, and to develop clinically useful metabolic indices of CNS involvement in seropositive subjects.

MATERIALS AND METHODS

Subjects

HIV-1 seropositive (HIV+) outpatients were recruited from neuroAIDS clinics at the Minneapolis VA Medical Center and the University of Minnesota Hospital. Twenty-one HIV+ subjects (20 men, 1 woman; aged 23–63 yr; mean age 43 ± 10 yr) were scanned at the Minneapolis VA Medical Center; 12 had a follow-up scan at 6 mo and 4 had a third scan at 12 mo. At the time of their initial scan, 11 subjects had AIDS. Four subjects were ADC Stage 0, twelve were Stage 0.5, four were Stage 1 and one was Stage 2 (11); one Stage 1 subject progressed to Stage 2, and two Stage 0.5 subjects "improved" to Stage 0. Of the 37 HIV+ scans, 11 were Stage 0, 18 were Stage 0.5 and 8 were Stage >0.5; there were no significant differences in age (42 ± 6, 43 ± 11, 50 ± 9 yr, respectively) or education (14 ± 2, 13 ± 2 and 15 ± 3 yr, respectively) across these groups.

All but 1 of the 21 subjects were male homosexuals or bisexuals. All but six of the HIV+ scans were performed while the subjects were taking zidovudine (AZT) and/or other antiviral drugs; eight subjects were taking tricyclic antidepressants. Subjects with a history of substance abuse, serious head injury, developmental disorder, or significant medical or psychiatric illness were specifically excluded. Prior to the study and at six-monthly follow-up visits, all subjects underwent a standardized neurologic and neuropsychological examination (*12*). Studies involving human sub-

Received Apr. 4, 1995; revision accepted Jul. 30, 1995.
For correspondence or reprints contact: D.A. Rottenberg, MD, PET Imaging Service (11P), VA Medical Center, One Veterans Drive, Minneapolis, MN 55417.

jects were approved by the Human Studies Subcommittee and the Radioactive Drug Research Committee at the Minneapolis VA Medical Center and by the Committee on Use of Human Subjects in Research at the University of Minnesota Hospital.

Forty-three volunteer heterosexual subjects (17 men, 26 women; age 21–80 yr; mean 46 ± 15 yr) served as normal controls (HIV−); five subjects were scanned twice at intervals ranging from 2 to 4 mo. Controls did not differ significantly from HIV+ subjects in age or education. All control subjects underwent a complete neurologic and standardized neuropsychological examination.

Patients and normal controls were evaluated with a series of neuropsychological tests sensitive to the characteristic deficits of ADC (*13,14*). The raw-score for an individual's performance on a particular test was converted to a Z-score, and a summary measure, the Neuropsychological Z-Score (NPZ Score), was derived by taking an average of the individual Z-scores.

MRI and Atrophy Assessment

For HIV+ subjects, diagnostic MRI [or, in four instances, CT] scanning was performed at the initial clinic visit to rule out unsuspected intracranial disease and repeated at 6 or 12 mo intervals. Ventricular and sulcal size was assessed visually by an experienced neuroradiologist (MJN) using T1- and T2-weighted images. Atrophy was rated on a scale of 0 (normal), 1+ (mild atrophy), 2+ (moderate atrophy) and 3+ (severe atrophy) with reference to age-matched normal controls. A composite Atrophy Score for each subject was calculated by averaging the ventricular and sulcal scores. The spacing between "paired" PET and MRI (CT) scans varied from zero (same day) to 51.1 wk (7.4 ± 11 wk, mean ± s.d.). Control subjects did not undergo MRI scanning.

PET

All patients and control subjects fasted overnight prior to receiving FDG (5 mCi/70 kg). Following the injection of tracer, serial PET images were acquired with the MVAMC ECAT 953B positron camera (*15*). The time course of plasma ^{18}F radioactivity was determined by sampling radial arterial blood and counting aliquots of plasma in a scintillation well-detector. Plasma glucose concentration was determined just before, during and after the 40-min dynamic scanning sequence. Reconstructed images corrected for random and scatter coincidences, tissue attenuation (transmission scan) and electronic deadtime effects were stored on optical disks and analyzed off-line. After reformatting the last frame of each 31-slice acquisition within a three-dimensional Talairach coordinate system (*16,17*), a standard set of 40 volumes of interest (VOIs)—36 (18/hemisphere) cortical and subcortical gray-matter (GM) VOI's, two cerebellar VOIs and two brainstem VOIs—were defined at specified Talairach coordinates (Table 1). CMRglc images were created from single 10-min frames and the time-course of arterial blood radioactivity using the Brooks modification of the Sokoloff-Phelps operational equation (*18–20*), individual subjects' GM rate constants k_1–k_3, $k_4 = 0$ and the lumped constant (LC) set equal to 0.52 (*21*).

PET Data Analysis

Rate Constants. Individual subjects' compartmental rate constants were compared for HIV+ and control groups using two-tailed t-tests.

Volumes of Interest. Each set of 40 VOIs was "replayed" on its respective CMRglc image. Peak regional CMRglc (rCMRglc) values were derived by averaging the upper 25% of functionalized VOI voxel values (*22*). Individual subject metabolic profiles, formed by plotting rCMRglc against VOI number were combined to form mean group profiles, which were compared using two-tailed t-tests and the Bonferroni correction for multiple comparisons.

Image Volumes. A voxel-based analysis (see Appendix) was performed in addition to the VOI-based analysis in order to demonstrate that the results obtained using VOIs were not simply a consequence of analyzing rCMRglc data from a particular subset of brain regions. The original dataset consisted of 85 image volumes (37 HIV+ and 48 controls). Of these, ten (six HIV+ and four controls) were discarded because the head was poorly positioned within the scanner's 10.8-cm axial field of view and the resulting images generated large-edge artifacts in the voxel-based analysis. Each of the remaining 75 volumes was converted into CMRglc units and a corresponding mask volume was created by thresholding each slice to exclude nonbrain voxels. Intersubject alignment parameters were then computed for each volume using a 12-parameter version of the ratio image uniformity method of Woods et al. (*23*) with a simulated PET volume in Talairach space serving as reference (*17*). Finally, the volumes were smoothed, reformatted in Talairach space and masked prior to Scaled Subprofile Model (SSM)/principal component analysis (PCA).

Scaled Subprofile Model/Principal Component Analysis. Pre- and post-PCA operations involving a logarithmic transformation followed by removal and estimation of: (1) a region-independent global scaling factor and (2) a regional pattern [or image volume] common to all subjects were performed as described by Moeller and Strother (*24*). This procedure is based on a variance partition into subject and region (VOI or voxel) terms and a residual equivalent to the interaction term of a two-way ANOVA (25, 26 and see Appendix). Singular value decomposition, which yields the same result as PCA (*25*), was performed on the data matrix with one subject's residual VOI or image voxels forming each row. This decomposed the residual matrix into uncorrelated eigenvectors and their associated principal component scores [or component images], which correspond to subject scaling factors (SSFs, subject weights) and offset relative group invariant subprofiles (GISs), respectively (24 and Appendix).

First- and second-eigenvector subject weights were regressed against the following independent measures: age, Atrophy Score, ADC Stage and NPZ Score. To control for Type I errors, we utilized a significance level of $p < 0.01$. In order to ascertain if the first two principal components were largely determined by one or a small number of severely affected outliers, a separate SSM/PCA analysis of the 16 subjects with ADC Stage <1 and 43 controls ("nonADC" subset) was performed, and the resultant eigenvectors, SSF1 and SSF2, and their respective principal component VOI profiles, GIS1 and GIS2, were regressed against the corresponding eigenvectors and GISs from the original 64-subject/85-scan analysis. A similar procedure was employed to rule out a significant effect of antidepressant medication ("no-antidepressants" subset).

Our VA Medical Center along with the Memorial Sloan-Kettering datasets—acquired more than 6 yr apart in different institutions with different PET scanners and stimulus conditions—were separately reanalyzed using a common set of 20 VOIs. The Minneapolis VA Medical Center dataset was also reanalyzed using the common set of VOIs after removal of the left and right cuneus (18-VOI analysis), and the SSFs for the first two principal components were predicted for all 12 ADC patients in the Memorial Sloan-Kettering dataset by projecting their VOI values onto the first and second GISs computed in the Minneapolis VA Medical Center analysis (*27*). Correlations with neuropsychological test scores for the Memorial Sloan-Kettering patients (Grooved Pegboard Dominant (GPD) and Grooved Pegboard Nondominant, (GPN)) were then obtained using the SSFs predicted for the second principal component [Fig. 2B in (*9*)].

TABLE 1
Talairach Coordinates (mm) of Standard Volumes of Interest

VOI	Region Name	x	y	z
1	L Cerebellum	−33.50	−66.80	−39.45
2	R Cerebellum	33.50	−66.80	−39.45
3	Pons	0.00	−25.60	−27.95
4	Midbrain	0.00	−22.85	−7.95
5	L Putamen	−23.12	2.07	5.74
6	R Putamen	23.12	2.07	5.74
7	L Caudate	−10.89	18.28	6.10
8	R Caudate	10.89	18.28	6.10
9	L Thalamus	−9.88	−15.33	10.54
10	R Thalamus	9.88	−15.33	10.54
11	L Inferior temporal gyrus	−52.60	−17.63	−20.64
12	R Inferior temporal gyrus	52.60	−17.63	−20.64
13	L Orbitofrontal gyrus	−53.94	−38.80	16.00
14	R Orbitofrontal gyrus	53.94	−38.80	16.00
15	L Hippocampus	−27.97	−24.40	−13.12
16	R Hippocampus	27.97	−24.40	−13.12
17	L Inferior frontal gyrus	−45.22	35.36	1.02
18	R Inferior frontal gyrus	45.22	35.36	1.02
19	L Anterior cingulate gyrus	−6.70	50.54	6.47
20	R Anterior cingulate gyrus	6.70	50.54	6.47
21	L Operculum	−51.42	3.97	7.68
22	R Operculum	51.42	3.97	7.68
23	L Cuneus	−6.20	−70.80	8.05
24	R Cuneus	6.20	−70.80	8.05
25	L Medial frontal gyrus	−26.97	55.20	8.23
26	R Medial frontal gyrus	26.97	55.20	8.23
27	L Transverse temporal gyrus	−44.39	−23.20	12.03
28	R Transverse temporal gyrus	44.39	−23.20	12.03
29	L Superior temporal gyrus	−53.94	−38.80	16.00
30	R Superior temporal gyrus	53.94	−38.80	16.00
31	L Precentral gyrus	−53.26	1.73	19.61
32	R Precentral gyrus	53.26	1.73	19.61
33	L Postcentral gyrus	−57.45	−14.03	19.98
34	R Postcentral gyrus	57.45	−14.03	19.98
35	L Posterior cingulate gyrus	−5.86	−49.40	20.44
36	R Posterior cingulate gyrus	5.86	−49.40	20.44
37	L Angular gyrus	−43.72	−58.60	34.59
38	R Angular gyrus	43.72	−58.60	34.59
39	L Supramarginal gyrus	−49.92	−49.60	34.87
40	R Supramarginal gyrus	49.92	−49.60	34.87

VOI = volume of interest; L = left; R = right.

RESULTS

Rate Constants and rCMRglc Values

GM rate constants k_1–k_3 were not significantly different in HIV+ and control subjects. Although HIV+ VOI means for caudate and putamen were higher than control means and the remaining 36 HIV+ VOI means were lower than control means (Fig. 1), these differences were not statistically significant.

Neuropsychological Testing

The NPZ Score was not correlated with age or education but declined significantly as a function of ADC Stage [$F(3,61) = 13.94$; $p < 0.0001$]. Post hoc (Student-Newman-Keuls) comparisons revealed that Stage >0.5 subjects performed significantly worse than each of the other groups and that Stage 0.5 subjects performed significantly worse than controls ($p < 0.0005$).

MRI and Atrophy Assessment

Aside from generalized cerebral atrophy (Fig. 2), MRI scans revealed only scattered white-matter lesions (T2 hyperintensities) in the most severely affected individuals. Composite Atrophy Scores ranged from zero (15 subjects) to 3.0 (two subjects) and averaged 0.90 (median 0.5).

SSM/PCA

The first two principal component VOI profiles—which account for 23% and 10% of the residual variance, respectively—and their subject weights are illustrated in Figure 3. Whereas cortical regions (VOI numbers > 10) are most heavily weighted in the first-component profile (GIS1), subcortical structures—the caudate, putamen and thalamus (VOIs 5–10)—are most heavily weighted in the second-component profile (GIS2, Fig. 3A). Not surprisingly, given the early-disease status (ADC Stage <1) of 16 of the 21 HIV+ subjects, HIV+ and control groups were not well separated along either eigenvector dimension (Fig. 3B).

In the voxel-based SSM/PCA analysis, only the sixth principal component demonstrated significant group differences at the $p < 0.001$ level (see Appendix); the SSFs for this component were significantly correlated with SSF2 from the VOI-based analysis ($r = 0.66$, $p < 10^{-6}$). The sixth principal

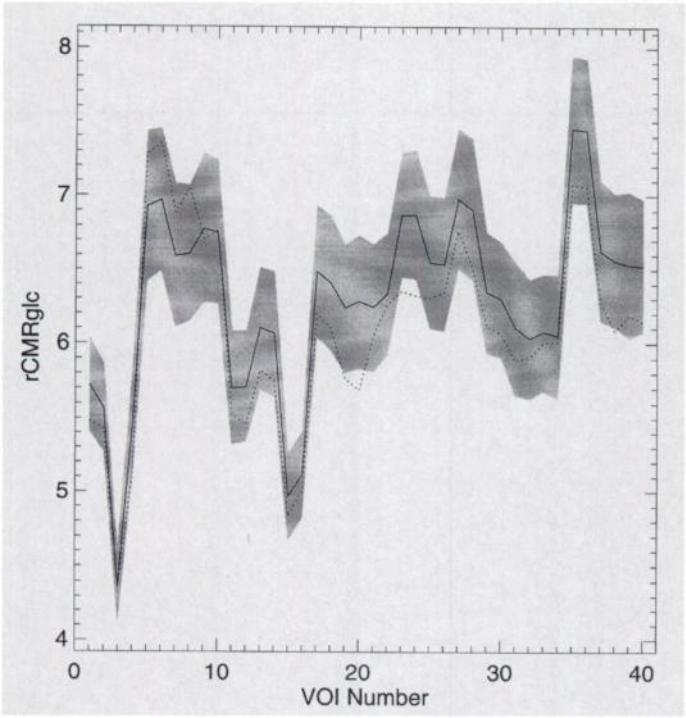

FIGURE 1. Comparison of mean regional metabolic rates in controls (solid line) and HIV+ subjects (dotted line). Shading indicates the 95% confidence limits on the difference between regional means. None of the HIV+ VOI values that lie outside these confidence limits is significantly different from controls when the confidence limits are Bonferroni-corrected for multiple comparisons. VOI Code: 1,2 L/R cerebellum; 3, pons; 4, midbrain; 5,6 L/R putamen; 7,8 L/R caudate; 9,10 L/R thalamus; 11,12 L/R inferior temporal gyrus; 13,14 L/R orbitofrontal gyrus; 15,16 L/R hippocampus; 17,18 L/R inferior frontal gyrus; 19,20 L/R anterior cingulate gyrus; 21,22 L/R operculum; 23,24 L/R cuneus; 25,26 L/R medial frontal gyrus; 27,28 L/R transverse temporal gyrus; 29,30 L/R superior temporal gyrus; 31,32 L/R precentral gyrus; 33,34 L/R postcentral gyrus; 35,36 L/R posterior cingulate gyrus; 37,38 L/R angular gyrus; 39,40 L/R supramarginal gyrus.

component image from the voxel-based SSM/PCA analysis is illustrated in Figure 4. As in GIS2 from the VOI-based analysis described above, the most heavily weighted voxels are located in the striata.

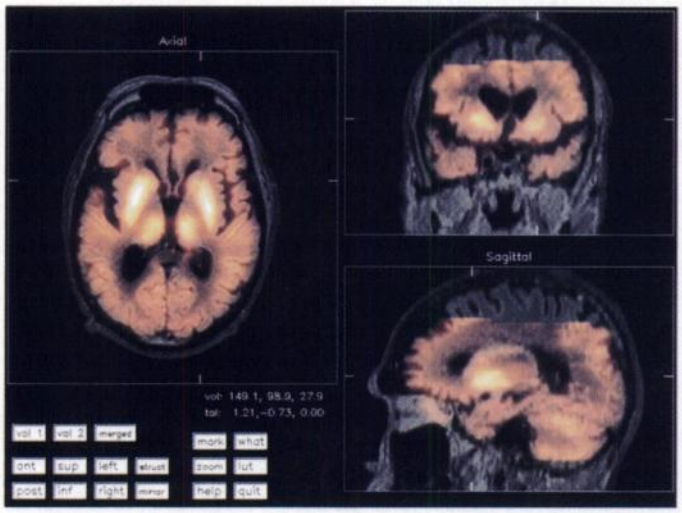

FIGURE 2. Merged display of registered MRI and FDG-PET volumes of a patient with Stage 2 ADC. Notice generalized cerebral atrophy and relative hypermetabolism in the putamina and thalami, the "metabolic signature" of ADC (*9*). The MRI image is displayed using a grayscale colortable, the interleaved PET image using a hot-metal color table [dull orange = low values, white = high values] (*32*).

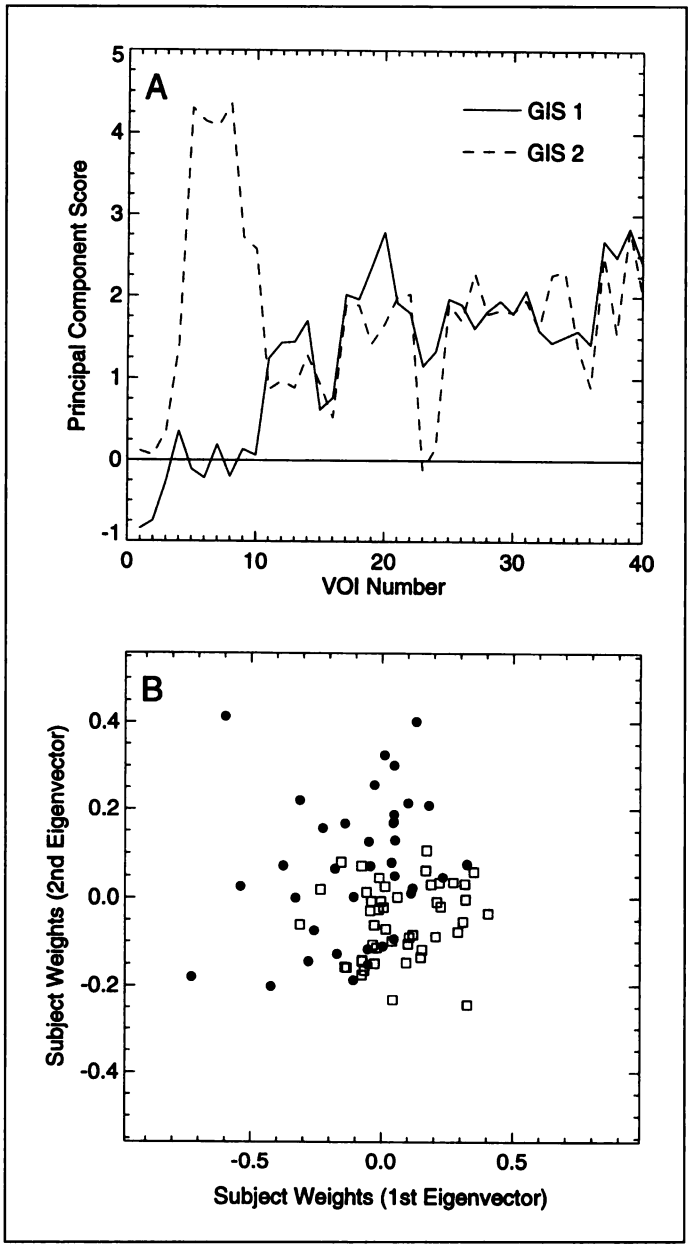

FIGURE 3. The first two PC VOI profiles and their eigenvectors (subject weights) derived by applying SSM/PCA to the combined HIV+ and controls dataset. (A) Scores for the first (solid line) and second (dashed line) PC VOI profiles are plotted against VOI number (see Fig. 1). (B) The second eigenvector of subject weights is plotted against the first eigenvector. Notice that HIV+ and control subjects cannot be separated along either eigenvector dimension. The first and second eigenvectors account for 23% and 10% of the residual variance, respectively.

The first two principal component VOI profiles from the separate analyses of the Minneapolis VA Medical Center and Memorial Sloan-Kettering datasets are compared in Figure 5. The patterns extracted from the two datasets are remarkably similar; however, VOIs 17 and 18 (left and right cuneus) are weighted differently in the Memorial Sloan-Kettering and Minneapolis VA Medical Center datasets. Correlations between SSF1, SSF2, GPD and GPN scores for Memorial Sloan-Kettering patients with AIDS Dementia Complex and predicted values based on the 18-VOI analysis of Minneapolis VA Medical Center HIV+ subjects are listed in Table 2.

The first and second eigenvectors of subject weights are plotted against age in Figure 6A, B, respectively. A strong interaction of HIV-serostatus with age is apparent in Figure 6A; the high Atrophy Scores for subjects older than 50 yr suggest

FIGURE 4. The sixth principal component image (see Appendix) from a voxel-based SSM/PCA analysis of 31 HIV+ and 44 control FDG-PET scans overlaid on a normal MRI scan. This principal component image illustrates a major area of altered functional connectivity associated with HIV-1 seropositivity and neurological/neuropsychological dysfunction.

that GIS1 reflects disease as well as age-dependent structural effects. Figure 6B illustrates a quantitatively different age effect: nearly half of the HIV+ subjects are metabolically abnormal, i.e., their subject weights are increased with respect to age-matched normal controls, and there is no obvious correlation with ADC Stage or Atrophy Score. The Fisher Discriminant (*28*), computed using the first two principal components from the SSM/PCA analysis, is illustrated in Figure 6C: 73% of HIV+ scans and 83% of control scans were correctly classified based on their Fisher Scores.

The relationship between NPZ Scores, subject weights for the first and second principal components from the VOI-based SSM/PCA analysis (SSF1, SSF2), Fisher Scores and disease severity (ADC Stage) is illustrated in Fig. 7. NPZ Scores for Stage 0.5 and >0.5 subjects and SSF1 weights for Stage >0.5 subjects were significantly different from controls (NPZ: $p < 0.0005$, $p < 0.00005$; SSF1: $p < 0.005$). SSF2 weights and Fisher Scores for Stage 0, Stage 0.5 and Stage >0.5 subjects differed significantly from controls (SSF2: $p < 10^{-6}$, $p < 0.01$ and $p = 0.01$; Fisher: $p < 10^{-6}$, $p < 0.0005$ and $p = 0.0006$).

First-eigenvector subject weights declined with ADC Stage (Fig. 7B) and were significantly correlated with age ($r = -0.69$, $p < 10^{-5}$ for HIV+; $r = -0.60$, $p < 10^{-5}$ for controls), Atrophy Score ($r = -0.58$, $p < 0.0005$) and ADC Stage ($r = -0.49$, $p < 0.005$). These correlations indicate that reduced cortical rCMRglc was associated with older age, cerebral atrophy and neurologic impairment. Second-eigenvector subject weights were uncorrelated with age, Atrophy Score, ADC Score or NPZ Score.

GIS1, SSF1, GIS2 and SSF2 from the original 64-subject analysis were highly correlated with the corresponding GISs and SSFs from the nonADC subset analysis ($r > 0.98$, $p < 10^{-6}$ for SSF1 and GIS1 regressions; $r > 0.90$, $p < 10^{6}$ for SSF2 and GIS2 regressions). A similar result was obtained from the no-antidepressants analysis ($r > 0.98$, $p < 10^{-6}$ for all four regressions).

DISCUSSION

The present study demonstrates characteristically altered patterns of metabolic covariation in HIV-seropositives, replicating the results of an earlier Memorial Sloan-Kettering study with a smaller group of more severely impaired patients. As in

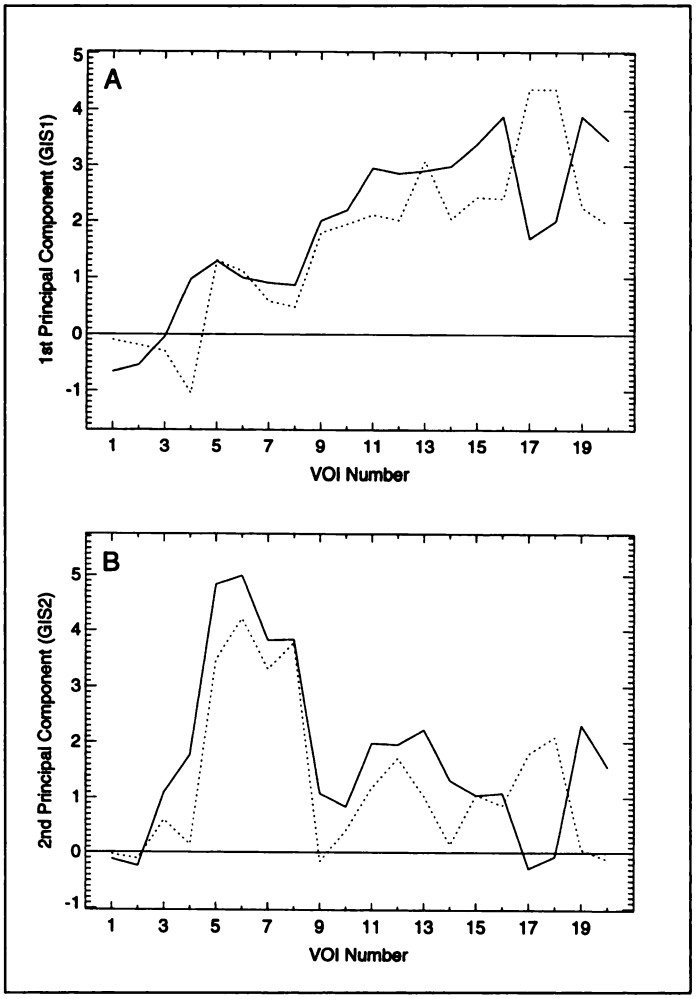

FIGURE 5. Comparison of SSM/PCA analyses of Minneapolis VA Medical Center HIV+ and Memorial Sloan-Kettering ADC datasets based on a common set of 20 VOIs (*9*). The first (A) and second (B) principal component scores are plotted against VOI number; solid lines refer to the Minneapolis VA Medical Center dataset, dashed lines to the Memorial Sloan-Kettering dataset (12 ADC patients, 18 controls).

our previous study, two disease-related principal components—which together accounted for 33% of the residual variance—were identified. GIS1 was most heavily weighted by cortical regions, and SSF1 was significantly correlated with age, cere-

TABLE 2
Correlations Between SSF1, SSF2, GPD and GPN Scores for Memorial Sloan-Kettering Patients with ADC and Predicted Values*

Correlation	r Value
MSK SSF1 vs. Predicted† MSK SSF1	0.968
MSK SSF2 vs. Predicted‡ MSK SSF2	0.945
MSK GPD scores vs. MSK SSF2	0.849
MSK GPD scores vs. Predicted‡ MSK SSF2	0.785
MSK GPN scores vs. MSK SSF2	0.819
MSK GPN scores vs. Predicted‡ MSK SSF2	0.762

*Based on an 18-VOI analysis of Minneapolis VA Medical Center HIV+ subjects.

†Predicted using GIS1 from the Minneapolis VA Medical Center analysis.

‡Predicted using GIS2 from the Minneapolis VA Medical Center analysis.

MSK = Memorial Sloan-Kettering; MVAMC = Minneapolis VA Medical Center; SSF = Subject Scaling Factor (see Appendix); GIS = Group Invariant Subprofile (see Appendix); GPD = Grooved Pegboard Dominant Hand; GPN = Grooved Pegboard Nondominant Hand.

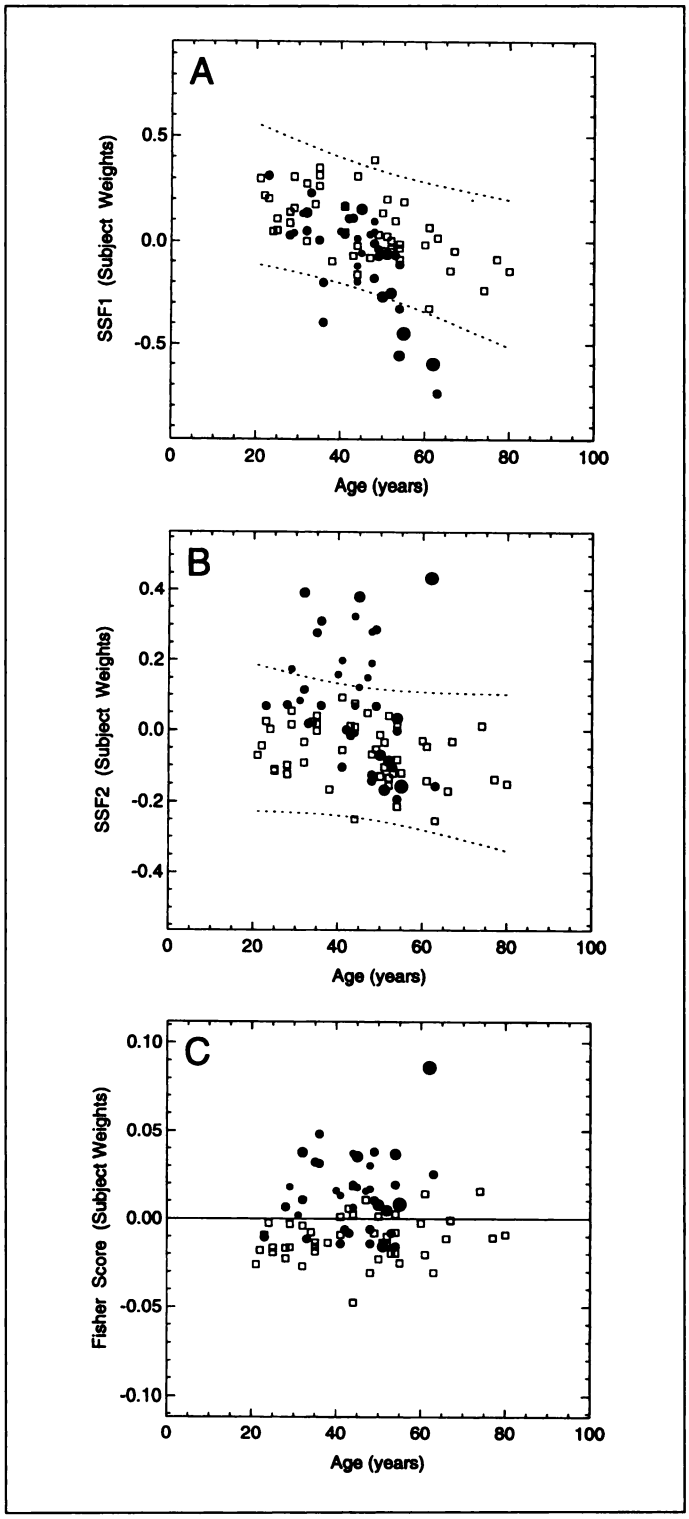

FIGURE 6. Age and disease dependency of eigenvector distributions and Fisher Scores. (A) The first eigenvector of subject weights from a SSM/PCA analysis of 37 HIV+ (solid symbols) and 48 normal control (open squares) scans is plotted against age. Circle radius is proportional to ADC stage. Dotted lines indicate 2 s.d. from the linear regression of control subject weights against age. Notice the more rapid falloff of subject weights with age for HIV+ subjects as compared to normal controls. (B) The second eigenvector of subject weights is plotted against age as in (A). Notice the large number of HIV+ outliers with positive subject weights that predict relative hypermetabolism in striatum and thalamus. Fisher scores derived from the first and second principal components are plotted against age in (C). The solid line parallel to the x-axis optimally discriminates HIV+ subjects and controls.

bral atrophy and neurological disability. GIS2 was heavily weighted by those subcortical regions identified as sites of HIV-1 infection, but SSF2 was not significantly correlated with independent measures of disease severity. We have previously shown that the GIS1 VOI profile is not specific for HIV+ and can be extracted from subjects with a variety of unrelated neurological disorders, and that different GIS2 VOI profiles are associated with different diseases (*29*).

Cross-Center Comparison

The 21 HIV+ subjects described in this report (Minneapolis series) differ in several important respects from the 12 ADC patients we reported in 1987 (Memorial Sloan-Kettering series). As a group, the Memorial Sloan-Kettering patients were younger than the Minneapolis subjects (37 ± 6 yr versus 43 ± 10 yr). Secondly—based on current CDC criteria—nine of the 12 Memorial Sloan-Kettering patients (75%) had AIDS at the time of study, whereas only 11 of the 21 Minneapolis subjects (52%) were so classified. Finally, and most importantly, ten of the 12 Memorial Sloan-Kettering patients were cognitively impaired, and nine were moderately-to-severely demented; in contrast, only three Minneapolis subjects were cognitively impaired at the time of initial study. Thus, in comparison to our Memorial Sloan-Kettering patients, the Minneapolis cohort represents an "early disease" group, systemically as well as neurologically.

Subcortical Hypermetabolism

In our 1987 paper, we hypothesized that relative subcortical hypermetabolism was characteristic of early ADC, whereas cortical and subcortical hypometabolism were the hallmarks of late-stage disease. The early-disease hypothesis has now been validated and extended in a larger group of HIV+ subjects—at another institution using a different PET scanner, stimulus condition and data extraction technique (Fig. 5). Moreover, the principal component VOI profiles and subject weights obtained from separate SSM/PCA analyses of nonADC and no-antidepressants subsets were highly correlated with the results of the original 64-subject analysis, indicating that the Minneapolis result does not depend upon the inclusion of a few severely-cognitively-impaired outliers or on the use of psychotropic medication. That most of the younger HIV+ "outliers" are neurologically normal suggests that positive weights on GIS2, which reflect relative subcortical hypermetabolism, may provide an indication of subclinical CNS disease.

In contrast to the Memorial Sloan-Kettering result, in which the eigenvector of subjects weights for the second principal component (SSF2) was highly correlated with independent measures of fine motor control, SSF2 from the Minneapolis analysis correlated poorly with measures of neurological disease severity (ADC Stage), fine motor control and cognitive impairment (NPZ Score). These poor correlations may reflect the relatively small number of HIV+ subjects in each ADC subgroup and/or the variability of our clinical, neuropsychological and metabolic measures in early disease. They may also indicate that the NPZ Score is more closely related to the primary source of systematic metabolic variation in our dataset, SSF1, a nonspecific marker for "neurologic disease" (*29*), than to SSF2, a putative marker for early HIV CNS disease. It is interesting to speculate that SSF2 reflects a restricted pathological process which precedes neurological signs and symptoms and which acquires a functional correlate when more widespread changes occur. While the second principal component accounted for only 10% of the residual variance, SSF2 and the SSM-derived global scaling factor, GSF (*24*), accurately predicted metabolic variation in the striatum: regressing rCMRglc/

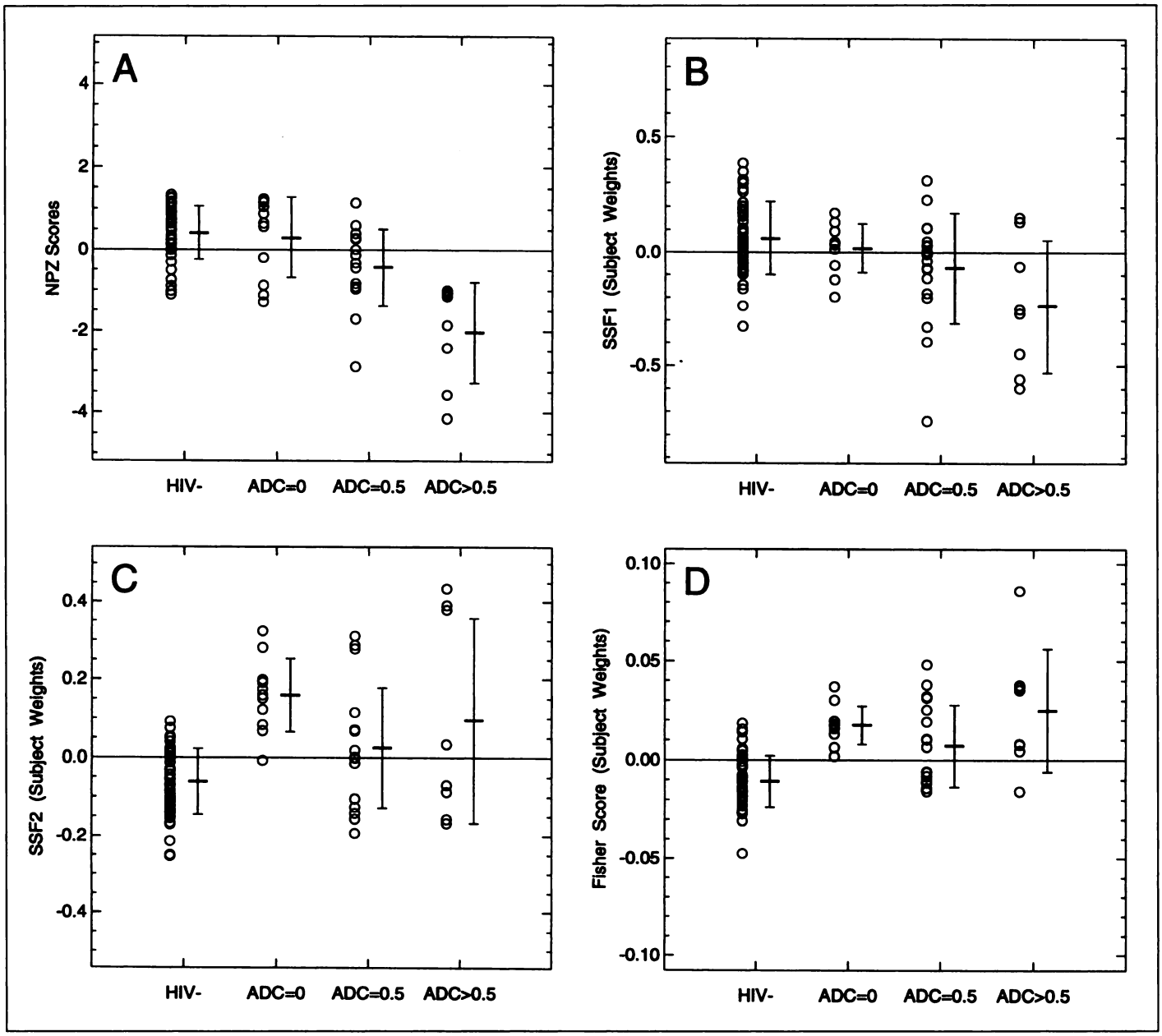

FIGURE 7. Relation between NPZ scores, subject weights for the first (SSF1) and second (SSF2) principal components from the VOI-based SSM/PCA analysis, Fisher scores derived from the first and second principal components and disease severity (ADC stage). NPZ scores (A), SSF1 and SSF2 subject weights (B,C) and Fisher scores (D) are plotted against ADC stage; error bars indicating 1 s.d. and a bold horizontal line indicating the group mean are plotted to the right of individual data points (open circles). "HIV−" refers to normal controls. Monotonic decrease in SSF1 weights (B) parallels the decrease in NPZ scores (A). SSF2 weights and Fisher scores for HIV+ subjects (C, D) are significantly greater than controls (SSF2: $p < 10^{-6}$, $p < 0.01$ and $p = 0.012$ for ADC Stage 0, Stage 0.5 and Stage > 0.5, respectively; Fisher scores: $p < 10^{-6}$, $p < 0.0005$ and $p < 0.001$).

GSF for left and right caudate and left and right putamen against SSF2 gave: $r = 0.87$, $r = 0.87$, $r = 0.88$ and $r = 0.90$, respectively; $p < 10^{-6}$. This result parallels that obtained from our Memorial Sloan-Kettering analysis and reinforces the interpretation of GIS2 as representing the metabolic effects of a network or system involved in the expression of ADC. Additional evidence for this interpretation derives from the fact that SSF1, SSF2, GPD and GPN for the Memorial Sloan-Kettering ADC patients were accurately predicted using GIS1 and GIS2 from the 18-VOI Minneapolis VA Medical Center analysis—even though only 5 of the 21 Minneapolis VA Medical Center HIV+ subjects had unequivocal ADC. These results provide further evidence that a disease-related network or system detected in one group of patients may be used to predict disease severity and/or progression in another, independent group across centers (*27*). That the putamen is so heavily weighted in the disease-related principal component VOI profile (GIS2, Fig. 3A) is hardly surprising in light of the neuropathology of ADC and its characteristic neurobehavioral manifestations.

Disease Progression

Our SSM/PCA results cannot be explained by cerebral atrophy, since focal atrophic lesions were not identified on CT or MRI scans. Moreover, it is difficult to understand how reduced basal ganglia volume might explain basal ganglia hypermetabolism (relative to normal controls). Assuming that basal ganglia atrophy implies neuronal loss, the presumed consequence of this loss would be hypometabolism; thus, the reduction in basal ganglia and thalamic rCMRglc in late disease (*9*) may reflect the progression of a focal atrophic process.

The most intriguing result of our analysis is illustrated in Figure 8, in which serial values of the second eigenvector of

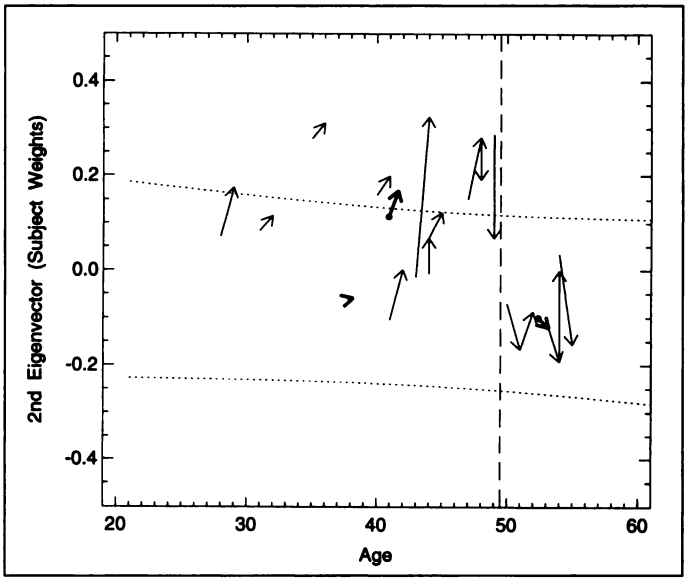

FIGURE 8. Vector plot of repeat FDG-PET scans. The second eigenvector of subject weights is plotted against age. Subjects scanned more than twice are represented as linked vectors. Dotted lines indicate two s.d. from the linear regression of control subject weights against age. A dashed line indicates the separation of the HIV+ group into two subgroups: age <50 yr and age ≥50 yr, each with an average vector (bold arrows). Whereas the near-zero magnitude of the average control vector (bold arrowhead) indicates that weights for control subjects are relatively constant over time, the average vector for HIV+ subjects <50 years of age indicates a tendency for subject weights to increase beyond the normal range (subcortical hypermetabolism).

subject weights (SSF2) are plotted as vectors for the 12 HIV+ subjects who were scanned more than once. Whereas the near-zero magnitude of the average control vector indicates that weights for control subjects are relatively constant over time, the average vector for HIV+ subjects less than 50 yr of age indicates a tendency for subject weights to increase beyond the normal range (subcortical hypermetabolism). The result illustrated in Figure 8 is consistent with the conclusion of Marder et al. (*30*) that neurologic impairment becomes increasingly apparent over time in HIV-seropositive men. Whether this result is attributable to neurologic or systemic disease—or to antiretroviral treatment, "lifestyle" or other, as-yet-undefined factors—is a subject for future investigation.

CONCLUSION

We replicated and extended the results of our FDG-PET study of the AIDS dementia complex and have demonstrated that metabolic principal component VOI profiles and their individual subject weights provide quantitative measures of abnormal functional connectivity in HIV+ subjects—with or without AIDS or ADC. These measures, which are robust across centers with respect to instrumentation, scanning technique, VOI definition and disease severity, appear to track the progression of CNS disease in patients with subclinical neurologic or neuropsychologic dysfunction. Additional studies will be required to assess their usefulness for predicting neurological deterioration and for monitoring treatment response.

APPENDIX

For a VOI-based analysis, the SSM model may be written as:

$$(\text{CMRglc})_{ij} = \text{GSF}_j(\text{GMP}_i + \text{SRP}_{ij}),$$

where

$$\text{SRP}_{ij} = \sum_{k=1}^{N} \text{SSF}_{kj}\text{GIS}_{ki}, \qquad \text{Eq. 1}$$

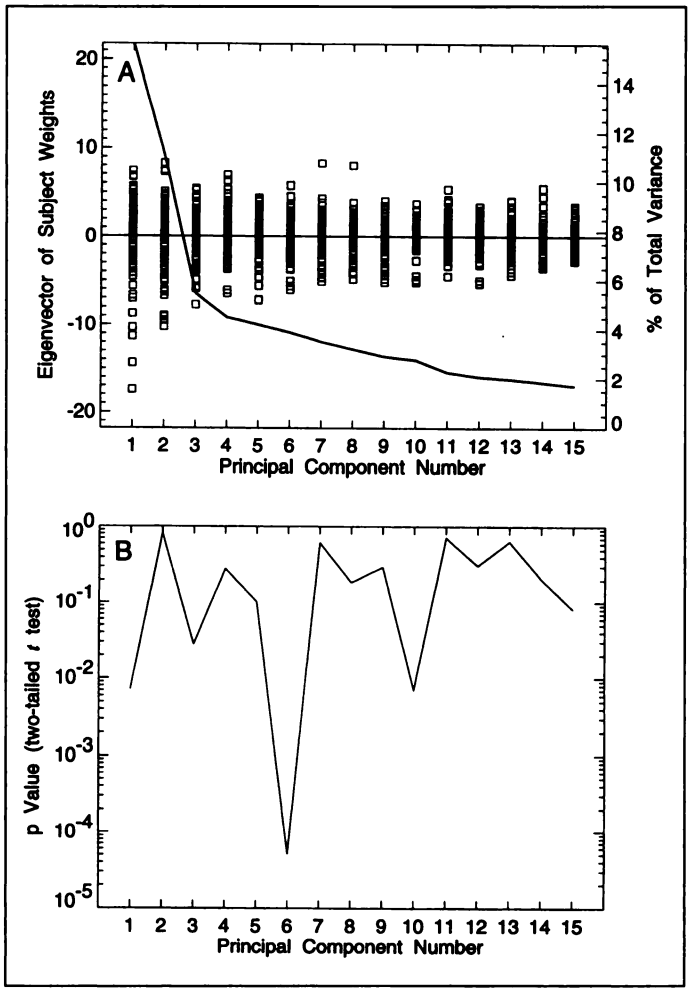

FIGURE 9. (A) The distribution of eigenvector subject weights (subject scaling factors, SSFs: open squares) for the first 15 principal components of the residual image volumes from a voxel-based SSM/PCA. Principal component variance is plotted as a percentage of the total subject residual image variance (solid line, right-hand ordinate). (B) p values obtained from two-tailed t-tests applied to the HIV+ and control group SSF distributions.

and j = subjects, i = VOIs, GSF = global scaling factor, GMP = group mean profile, SRP = subject residual profile (containing subject-region interactions and inherent error), SSF = subject scaling factor, GIS = group invariant subprofile and N = min(# subjects, # VOIs) (*24*). For a voxel-based analysis, replace the word *profile* above with the words *image volume*, and *VOIs* with *voxels*. A logarithmic (ln) transformation is applied to the $(\text{CMRglc})_{ij}$ data, which, using the small signal approximation $\ln(1 + x) \approx x$ for $x \ll 1$, provides a two-way randomized blocks ANOVA decomposition (*31*) with the interaction and error terms represented by $(\text{SRP}_j/\text{GMP})_i$:

$$\ln(\text{CMRglc})_{ij} \approx \ln(\text{GSF})_j + \ln(\text{GMP})_i + \left(\frac{\text{SRP}_j}{\text{GMP}}\right)_i. \qquad \text{Eq. 2}$$

After double centering of the $\ln(\text{CMRglc})_{ij}$ data matrix (subtraction of row means followed by subtraction of column means of the row-subtracted data) to remove subject and region main effects, the resulting offset relative residual term (left side of Eq. 3) is decomposed into eigenvectors of subject weights (SSFs) and principal component scores—offset-relative VOI profiles or image volumes—(right side of Eq. 3) using SVD (*25*). Double centering of Equation 2 followed by substitution of SRP from Equation 1 gives the following formula:

$$\left(\frac{SRP_j}{GMP}\right)_i - \left(\frac{SRP_j}{GMP}\right)_\cdot = \sum_{k=1}^{K} SSF_{kj}\left[\left(\frac{GIS_k}{GMP}\right)_i - \left(\frac{GIS_k}{GMP}\right)_\cdot\right] + e_{ij} \quad (\because SRP_{i\cdot} = 0), \qquad \text{Eq. 3}$$

where K = (number of retained principal components) $\ll$ min(# subjects, # voxels or VOIs) and the error term, e_{ij}, is represented by the N − K remaining principal components. Multiple regression of $\ln(CMRglc)_{\cdot j}$ against the K × SSF_{kj}'s (substitute SRP from Eq. 1 into Eq. 2) provides estimates of the K × $(GIS_k/GMP)_\cdot$ offsets (regression coefficients) and the $\ln(GSF)_j$ (residuals). The GSFs are then used to estimate GMP_i, which, together with the K offsets, is used to estimate the K × GIS_{ki}'s (*24*).

For both the 85-scan VOI analysis and the voxel-based analysis of 75 image volumes (see Materials and Methods), K was chosen to include all PCs (from the first fifteen) up to the PC for which the groups of HIV+ and normal SSFs were significantly different ($p < 0.05$, two-tailed t-test). This gave K = 6 and K = 10 for VOIs and voxels, respectively. Figure 9 illustrates the eigenspectrum of the first 15 components and their associated group difference p values for the voxel-based analysis. Only Component 6 exhibits significant group differences ($p < 0.001$).

Features of the "striatal pattern" in Component 2 of the VOI-based analysis have migrated to Component 6 of the voxel-based analysis as a result of additional sources of intersubject variability from uncorrelated structural and functional components introduced by the much larger number of regional measurements—22,682 voxels versus 40 VOIs. The relationship between VOI and voxel-based patterns is an important area for future research.

ACKNOWLEDGMENTS

We thank Dr. J. Thurn for patient referrals, Mss. D. Daly, C. Farmer and D. Hamm for invaluable technical assistance, and Dr. K. Rehm for producing the computer graphics. This work was supported by National Institutes of Health grants NS25701, NS25563 and NS33718.

REFERENCES

1. Albert ML, Feldman RG, Willis AL. The "subcortical dementia" of progressive supranuclear palsy. *J Neurol Neurosurg Psychiat* 1974;37:121–130.
2. Cummings JL, Benson DF. Subcortical dementia: review of an emerging concept. *Arch Neurol* 1984;41:874–879.
3. Navia BA, Jordan BD, Price RW. The AIDS dementia complex: I. Clinical features. *Ann Neurol* 1986;19:517–524.
4. Price RW, Brew B, Sidtis J, Rosenblum M, Scheck AC, Cleary P. The brain in AIDS: central nervous system HIV-1 infection and AIDS dementia complex. *Science* 1988;239:586–592.
5. Navia BA. The AIDS dementia complex. In: Cummings JL, ed. *Subcortical dementia*. New York: Oxford University Press; 1990:181–198.
6. Navia BA, Cho ES, Petito CK, Price RW. The AIDS dementia complex: II. Neuropathology. *Ann Neurol* 1986;9:525–535.
7. Lantos PL, McLaughlin JE, Scholtz CL, Berry CL, Tighe JR. Neuropathology of the brain in HIV infection. *Lancet* 1989;1:309–311.
8. Budka H. Neuropathology of human immunodeficiency virus infection. *Brain Pathol* 1991;1:163–175.
9. Rottenberg DA, Moeller JR, Strother SC, et al. The metabolic pathology of the AIDS dementia complex. *Ann Neurol* 1987;22:700–706.
10. van Gorp WG, Mandelkern MA, Gee M, Hinkin CH, et al. Cerebral metabolic dysfunction in AIDS: findings in a sample with and without dementia. *J Neuropsychiat* 1992;4:280–287.
11. Price RW, Brew BJ. The AIDS dementia complex. *J Infect Dis* 1988;158:1079–1083.
12. Price RW, Sidtis JJ. Evaluation of the AIDS dementia complex in clinical trials. *J AIDS* 1990;3(suppl 2):S51–S60.
13. Sidtis JJ, Gatsonis C, Price RW, et al. Zidovudine treatment of the AIDS dementia complex: results of a placebo-controlled trial. *Ann Neurol* 1993;33:343–349.
14. Sidtis, JJ. Evaluation of the AIDS dementia complex in adults. In: Price RW, Perry SW, eds. *HIV, AIDS and the Brain*. New York: Raven Press; 1994:273–287.
15. Spinks TJ, Jones T, Bailey DL, et al. Physical performance of a positron tomograph for brain imaging with retractable septa. *Phys Med Biol* 1992;37:1637–1655.
16. Talairach J, Tournoux P. *Co-planar stereotaxic atlas of the human brain*. New York: Thieme Medical Publishers; 1988.
17. Strother SC, Anderson JR, Xu X-L, Liow J-S, Bonar DC, Rottenberg DA. Quantitative comparisons of image registration techniques based on high-resolution MRI of the brain. *J Comput Assist Tomogr* 1994;18:954–962.
18. Sokoloff L, Reivich M, Kennedy C, et al. The [^{14}C]deoxyglucose method for the measurement of local cerebral glucose utilization: theory, procedure and normal values in the conscious and anesthetized albino rat. *J Neurochem* 1977;28:897–916.
19. Phelps ME, Huang SC, Hoffman EJ, Selin C, Sokoloff L, Kuhl DE. Tomographic measurement of local cerebral glucose metabolic rate in humans with [^{18}F]2-fluoro-2-deoxy-D-glucose. Validation of method. *Ann Neurol* 1979;6:371–388.
20. Brooks RA. Alternative formula for glucose utilization using labeled deoxyglucose. *J Nucl Med* 1982;23:538–539.
21. Reivich M, Alavi A, Wolf A, et al. Glucose metabolic rate kinetic model parameter determination in humans: the lumped constants and rate constants for [^{18}F]fluorodeoxyglucose and [^{11}C]deoxyglucose. *J Cereb Blood Flow Metab* 1985;5:178–192.
22. Rottenberg DA, Moeller JR, Strother SC, Dhawan V, Sergi ML. Effects of percent thresholding on the extraction of [^{18}F]fluorodeoxyglucose positron emission tomographic region of interest data. *J Cereb Blood Flow Metab* 1991;11:A83–A88.
23. Woods RP, Mazziotta JC, Cherry SR. Automated image registration. In: Uemura K, Lassen NA, Jones T, Kanno I, eds. *Proceedings of brain PET '93 AKITA: quantification of brain function*. Amsterdam: Excerpta Medica; 1993;391–398.
24. Moeller JR, Strother SC. A regional covariance approach to the analysis of functional patterns in positron emission tomographic data. *J Cereb Blood Flow Metab* 1991;11: A121–A135.
25. Jackson JE. A user's guide to principal components. New York: John Wiley; 1991.
26. Gollob HF. A statistical model which combines features of factor analytic and analysis of variance techniques. *Psychometrika* 1968;38:555–569.
27. Eidelberg D, Moeller JR, Ishikawa T, et al. Assessment of disease severity in Parkinsonism with fluorine-18-fluorodeoxyglucose and PET. *J Nucl Med* 1995;36: 378–383.
28. Mardia KV, Kent JT, Bibby JM. *Multivariate Analysis*. New York: Academic Press; 1989:318–320.
29. Strother SC, Moeller JR, Sidtis JJ, Rottenberg DA. Using principal component analysis to identify a disease independent pattern of cerebral metabolic activation: the reticular activating system? In: Uemura K, Lassen NA, Jones T, Kanno I, eds. *Proceedings of brain PET '93 AKITA: quantification of brain function*. Amsterdam: Excerpta Medica; 1993:491–495.
30. Marder K, Liu X, Stern Y, et al. Neurologic signs and symptoms in a cohort of homosexual men followed for 4.5 yr. *Neurology* 1995;45:261–267.
31. Snedecor GW, Cochran WG. *Statistical methods*, 7th ed. Ames: Iowa State University Press; 1980.
32. Rehm K, Strother SC, Anderson JR, Schaper K, Rottenberg DA. Display of merged multimodality brain images using interleaved pixels with independent color scales. *J Nucl Med* 1994;35:1815–1821.